Acta Crystallographica Section A
Foundations of Crystallography
ISSN 0108-7673

Received 10 December 2008
Accepted 29 January 2009

Correcting electron-density resolution bias in reciprocal space

Angela Altomare,[a] Corrado Cuocci,[a] Carmelo Giacovazzo,[a,b]* Sabino Maggi,[a] Anna Moliterni[a] and Rosanna Rizzi[a]

[a]Istituto di Cristallografia, Sede di Bari, Via G. Amendola 122/o, 70126 Bari, Italy, and [b]Dipartimento Geomineralogico, Università di Bari, Campus Universitario, Via Orabona 4, 70125 Bari, Italy. Correspondence e-mail: carmelo.giacovazzo@ic.cnr.it

Fourier syntheses are always affected by series-termination errors, which generate sets of positive and negative ripples around each main peak in the map. The interaction among the ripples distorts the profile of the map and moves peaks away from their correct positions. In a previous paper [Altomare *et al.* (2008). *Acta Cryst.* A**64**, 326–336] an algorithm was described which reduces the resolution bias by removing the effects of the ripples in direct space. In this paper the correction is performed in reciprocal space: the effect of the ripples on the atomic scattering factors is calculated and subtracted from the usual atomic scattering factors. The modified scattering factors are used to calculate new structure factors, from which more accurate electron-density maps may be obtained. The experimental tests show that the procedure minimizes the effects of the resolution bias and provides atomic positions that are more accurate than those provided by traditional approaches.

1. Introduction

One of the major limitations in modern crystallography is the experimental data resolution (RES). In macromolecular crystallography RES is rarely atomic (*i.e.* 1 Å or better), and usually ranges from tens of angströms to ~2 Å. When only powder data are available, high-resolution measurements are often of limited use, particularly for organic structures: this is partly due to the decay of the atomic scattering and partly to peak overlap, which limits the accuracy of the full pattern decomposition. It is not uncommon for even single-crystal data for small molecules to not extend to atomic resolution due to the low perfection of the crystal samples.

When RES > 1 Å, both phasing and refinement processes are difficult. In particular, the electron density obtained as the Fourier transform of the structure factors shows series-termination errors: as a consequence, the map is negative in some regions, and peaks are broadened and surrounded by positive and negative ripples. The map is then an imperfect representation of the true electron density.

Let

$$\rho(\mathbf{r}) = \sum_{j=1}^{N} \rho_j(\mathbf{r} - \mathbf{r}_j)$$

be the true electron density, describing a crystal structure of N atoms in the unit cell, and let $F_{\mathbf{h}}$ be its generic structure factor. If $\Phi(\mathbf{r}^*)$ is the shape function of the measurable domain of the reciprocal space [$\Phi(\mathbf{r}^*) = 1$ inside the measured domain, $\Phi(\mathbf{r}^*) = 0$ outside it], then the structure factors available experimentally are

$$F'_{\mathbf{h}} = F_{\mathbf{h}}\Phi(\mathbf{r}^*) \tag{1}$$

and, correspondingly, the electron-density map $\rho'(\mathbf{r})$ computable in practice is

$$\rho'(\mathbf{r}) = \rho(\mathbf{r}) \otimes T[\Phi(\mathbf{r}^*)] = \rho(\mathbf{r}) \otimes \zeta(\mathbf{r}) = \sum_{j=1}^{N} \rho_j(\mathbf{r} - \mathbf{r}_j) \otimes \zeta(\mathbf{r}) = \sum_{j=1}^{N} \rho'_j(\mathbf{r} - \mathbf{r}'_j), \tag{2}$$

where $\zeta(\mathbf{r})$ is the Fourier transform of $\Phi(\mathbf{r}^*)$ and $\otimes$ denotes the convolution operation. The maximum of $\rho'_j(\mathbf{r})$ will be located at a position $\mathbf{r}'_j$, usually non-coincident with the position $\mathbf{r}_j$. The effects of the series-termination errors on the electron-density maps were well known even in the early years of modern crystallography. In particular, Booth (1946) addressed his attention to the upper limits of the positional errors for atoms in very simple structures. Cruickshank (1949) investigated the variance in electron-density maps, generated by measurement errors and series-termination errors. His results were generalized by Rees (1976), who derived an expression for the covariance between densities at two points of the electron-density map by taking into account the experimental data resolution. Nowadays the most popular way of overcoming the resolution bias is to calculate difference electron densities: they are less sensitive to series-termination effects but provide only models for the difference structure.

Quite recently, two papers [Altomare, Cuocci, Giacovazzo, Kamel *et al.* (2008) and Altomare, Cuocci, Giacovazzo, Moliterni & Rizzi (2008), from now on referred to as papers I and II] proposed a new practical approach for the resolution-bias correction. In paper I the mathematical bases of the

method, relying on diffraction physics, were stated. They require the generalization of the traditional concept of a Gaussian-like peak: each jth atomic peak is replaced by a two-component function, extending over the full unit cell, comprising the *main peak* and the corresponding ripples. Each component of the generalized peak is mathematically modelled in the corresponding existence domain: *e.g.*, the jth main peak has its own existence domain (say $[A]_j$), while the ripples extend over all the rest of the unit cell (say, the domain $[B]_j$). Accordingly, each peak $\rho'_j(\mathbf{r}-\mathbf{r}'_j)$ is represented as the sum of two functions:

$$\rho'_j(\mathbf{r}-\mathbf{r}'_j) = \rho'_{[A]_j}(\mathbf{r}-\mathbf{r}'_j) + \rho'_{[B]_j}(\mathbf{r}-\mathbf{r}'_j), \tag{3}$$

where $\rho'_{[A]_j}(\mathbf{r}-\mathbf{r}'_j)$ is defined in $[A]_j$, and represents the jth main peak, while $\rho'_{[B]_j}(\mathbf{r}-\mathbf{r}'_j)$, defined in $[B]_j$, describes its ripples.

Moreover, the oscillating function $\zeta(\mathbf{r})$ is represented as a two-component function, according to the following definitions: (*a*) d_ζ is the distance from the origin of the first $\zeta(\mathbf{r})$ zero point; (*b*) $[A]_\zeta$ is the collection of points $\mathbf{r}$ for which $|\mathbf{r}| \leq d_\zeta$; (*c*) $[B]_\zeta$ is the rest of the unit cell; (*d*) $\zeta_{[A]\zeta}$ and $\zeta_{[B]\zeta}$ are the parts of the function $\zeta(\mathbf{r})$ corresponding to the domains $[A]_\zeta$ and $[B]_\zeta$, respectively. According to paper II, the resolution-bias algorithm finds a more appropriate representation of the electron density [say $\rho'_{\rm mod}(\mathbf{r})$] starting from the experimental electron density $\rho'(\mathbf{r})$. The algorithm works in direct space and may be described as follows:

(i) ripple effects are eliminated from the function $\rho'(\mathbf{r})$, giving rise to the intermediate function

$$\rho''(\mathbf{r}) = \rho'(\mathbf{r}) - \sum_{j=1}^{N} \rho'_{[B]j}(\mathbf{r}-\mathbf{r}'_j) \approx \sum_{j=1}^{N} [\rho'_j(\mathbf{r}-\mathbf{r}'_j) - c'_j \zeta_{[B]_\zeta}(\mathbf{r}-\mathbf{r}'_j)], \tag{4}$$

where $c'_j = \rho'(\mathbf{r}'_j)/\zeta(0)$ is a scaling factor. The main maxima of $\rho''(\mathbf{r})$ are centred on $\mathbf{r}''_j$.

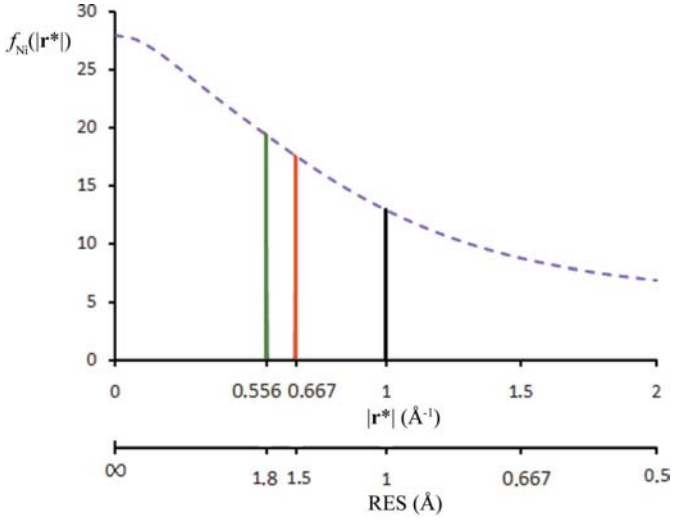

Figure 1
$f_{\rm Ni}$ *versus* $|\mathbf{r}^*|$ and RES at $B = 0$ Å^2. The sharp vertical lines correspond to three different $\Phi(\mathbf{r}^*)$ limits (RES = 1.0, 1.5 and 1.8 Å are shown in black, red and green, respectively).

(ii) Each main peak $\rho''_{[A]_j}(\mathbf{r}-\mathbf{r}''_j)$ is considered to be the convolution of $\rho_j(\mathbf{r}-\mathbf{r}''_j)$ with $\zeta_{[A]_\zeta}(\mathbf{r})$:

$$\rho''_{[A]_j}(\mathbf{r}-\mathbf{r}''_j) \approx \rho_j(\mathbf{r}-\mathbf{r}''_j) \otimes \zeta_{[A]_\zeta}(\mathbf{r}). \tag{5}$$

(iii) Both functions on the right-hand side of equation (5) are approximated by Gaussian functions: accordingly their convolution $\rho''_{[A]j}(\mathbf{r}-\mathbf{r}''_j)$ may also be approximated by a Gaussian function and therefore the desired function $\rho'_{\rm mod}(\mathbf{r})$ may be written as

$$\rho'_{\rm mod}(\mathbf{r}) \approx \sum_{j=1}^{N} c_j G(\mathbf{r}; \sigma_j, \mathbf{r}''_j). \tag{6}$$

The algorithm is able to estimate the parameters c_j and σ_j as a function of RES. It was implemented in a modified version of *EXPO2004* (Altomare *et al.*, 2004) and applied to a set of test structures, most of which were organic with RES > 1 Å, and which were originally solved by *DASH* (David *et al.*, 2001) *via* simulated-annealing techniques given prior information on the molecular geometry. The resolution-bias correction allowed *EXPO2004* to solve most of them *via* direct methods, without any use of the molecular geometry information. In the absence of a resolution-bias correction, most of the above structures were absolutely resistant to any attempt to solve them using *EXPO2004*. This paper describes a different algorithm, also aimed at minimizing the resolution bias, but working in reciprocal space, through the resolution-dependent modification of the atomic scattering factors. The new algorithm is successfully applied to simulated cases and to a real structure.

2. The algorithm

The proposal of an algorithm for correcting resolution bias in reciprocal space implies a positive answer to the following questions: may an electron-density map calculated *via* modified (resolution-dependent) structure factors show truncation effects smaller than in the canonical electron-density map? May it also locate peaks more appropriately? If so, such a map would display interesting features both in the phasing and in the refinement steps of the crystal structure analysis.

Let us rewrite equation (1) as follows:

$$F'_{\mathbf{h}} = F_{\mathbf{h}} \Phi(\mathbf{r}^*) = \sum_{j=1}^{N} f'_j(|\mathbf{r}^*|) \exp(2\pi i \mathbf{h}\cdot\mathbf{r}_j),$$

where

$$f'_j(|\mathbf{r}^*|) = f_j(|\mathbf{r}^*|)\Phi(\mathbf{r}^*).$$

In general, f_j includes the thermal factor B: for the sake of simplicity, in this and in the next section we will assume $B = 0$ Å^2. The difference between $f'_j(|\mathbf{r}^*|)$ and $f_j(|\mathbf{r}^*|)$ is shown in Fig. 1 for Ni at $B = 0$ Å^2, for three different definitions of $\Phi(\mathbf{r}^*)$. The three cutoff values (at $|\mathbf{r}^*| = 0.556$, 0.667 and 1.0 Å^{-1}) imply that all the scattering factors f' vanish for RES < 1.8, 1.5 and 1.0 Å, respectively. Correspondingly, the structure factors will also vanish outside such limits.

Let us calculate the Fourier transform of $f_{\rm Ni}$ and $f'_{\rm Ni}$ at B = 0 Å^2. According to Doyle & Turner (1968), any atomic scattering factor may be represented as a constant plus the sum of four Gaussian functions:

$$f_j(|\mathbf{r}^*|) = c + \sum_{i=1}^{4} a_i \exp(-b_i \cdot |\mathbf{r}^*|^2/4).$$

Its Fourier transform $\rho_{\rm Ni}(|\mathbf{r}|)$ will represent the electron distribution in the domain occupied by the Ni atom. In Fig. 2 $\rho_{\rm Ni}(|\mathbf{r}|)$ is shown by a dashed purple line. If the Fourier transform of $f'_{\rm Ni}(|\mathbf{r}^*|)$ is calculated at RES = 1.8, 1.5 and 1.0 Å, respectively, the curves $\rho'_{\rm Ni}(|\mathbf{r}|)$ are obtained (the green, red and black lines, respectively). The presence of ripples suggests that the resolution cutoff on the scattering factor is the primary source of their occurrence: they are also not negligible when RES = 1 Å.

Let us now return to a general crystal structure with N atoms in the unit cell, for which a molecular model is available. In order to minimize the resolution-bias effects present in $\rho'(\mathbf{r})$ we calculate the inverse Fourier transform of equation (4). For simplicity we first eliminate the scaling factor c'_j from the calculations: that is obtained by estimating $f_{[B]_\zeta \mathbf{h}}$ for each atomic species present in the crystal (*i.e.*, *via* Fourier transform of the ripple function $\zeta_{j[B]_\zeta}$ related to each atomic species). We obtain

$$F''_{\mathbf{h}} = F'_{\mathbf{h}} - F_{[B]_\zeta \mathbf{h}}, \tag{7a}$$

where

$$F''_{\mathbf{h}} = T^{-1}[\rho''(\mathbf{r})], \tag{7b}$$

$$F'_{\mathbf{h}} = T^{-1}[\rho'(\mathbf{r})] = \sum_{j=1}^{N} f'_j \exp(2\pi i \mathbf{h} \cdot \mathbf{r}'_j), \tag{7c}$$

$$F_{[B]_\zeta \mathbf{h}} = T^{-1}\left[\sum_{j=1}^{N} \zeta_{j[B]_\zeta}(\mathbf{r} - \mathbf{r}'_j)\right] = \sum_{j=1}^{N} f_{j[B]_\zeta \mathbf{h}} \exp(2\pi i \mathbf{h} \cdot \mathbf{r}'_j) \tag{7d}$$

and

$$f_{j[B]_\zeta} = T^{-1}[\zeta_{j[B]_\zeta}].$$

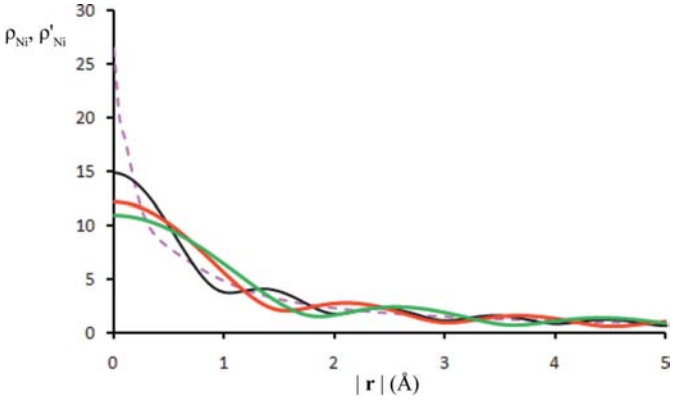

Figure 2
$\rho_{\rm Ni}(\mathbf{r})$ (dashed purple line) at B = 0 Å^2. The $\rho'_{\rm Ni}(\mathbf{r})$ curves obtained at RES = 1.8, 1.5 and 1.0 Å are shown in black, red and green, respectively.

In accordance with equation (4) an electron density corrected for the resolution bias should be computed *via* the coefficients

$$F''_{\mathbf{h}} = \sum_{j=1}^{N} [f'_j - f_{j[B]_\zeta \mathbf{h}}] \exp(2\pi i \mathbf{h} \cdot \mathbf{r}'_j). \tag{8}$$

It is expected that using $f''_j = (f'_j - f_{j[B]_\zeta \mathbf{h}})$ rather than f'_j in the structure-factor calculation may lead, after the Fourier transform, to an improved electron-density map. Since $\zeta_{[B]_\zeta}(\mathbf{r})$ is centrosymmetric (*i.e.*, it takes equal values in $\mathbf{r}$ and in $-\mathbf{r}$) its Fourier transform $f_{[B]_\zeta}$ will assume real (positive or negative) values.

In Fig. 3 $f_{{\rm Ni}[B]_\zeta}$ is shown for RES = 1.8, 1.5 and 1.0 Å (the green, red and black lines, respectively). In the interval $|\mathbf{r}^*|$ = 0.1 to 1/RES it increases continuously with $|\mathbf{r}^*|$ (the discontinuity edges occur at $|\mathbf{r}^*|$ = RES^{-1}: the edges and the intervals after them will be commented on in §3): it is negative at low resolution and positive for higher-resolution reflections. Its zero point decreases for increasing values of RES.

In Fig. 4 $f''_{\rm Ni}$ is shown for RES = 1.8, 1.5 and 1.0 Å (the green, red and black lines, respectively) (the behaviour of $f''_{\rm Ni}$ beyond RES will be commented on in §3). In the same figure, for comparison, $f_{\rm Ni}$(dashed line) is plotted *versus* $|\mathbf{r}^*|$ up to RES = 1 Å. We note:

(i) The overall effect of the algorithm is to increase the scattering amplitude at low $|\mathbf{r}^*|$ values and decrease it at high values. In particular, the value of $f''_{\rm Ni}$ at $|\mathbf{r}^*| = 0$ is larger than the atomic number of Ni (*i.e.*, larger than Z = 28).

(ii) The sharpening of the scattering factor is RES dependent: as a consequence, the form of the atomic peak obtained by the Fourier transform of $f''_{\rm Ni}$ will also be RES dependent: in particular it will be smoother after the resolution-bias correction.

(iii) The algorithm modifies the form of f'_j by slightly reducing its overall scattering power. Indeed, the integral of $f_{{\rm Ni}[B]_\zeta}$ is close to zero for any practical value of RES (see Fig. 3).

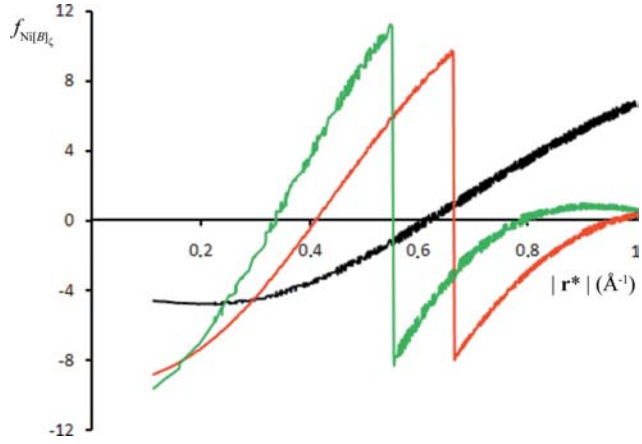

Figure 3
$f_{{\rm Ni}[B]_\zeta}$ (at B = 0 Å^2) extended to RES = 1.0 Å where the curves obtained for RES = 1.0, 1.5 and 1.8 Å are shown in black, red and green, respectively.

The above considerations indicate that the resolution-bias-correction algorithm associates smaller scattering factors with high-resolution reflections and larger scattering factors with low-resolution reflections. That is not equivalent to the effects of thermal vibration, which depletes the scattering factors of all the reflections, with larger effects for the high-resolution reflections. This difference is the key for the success of the resolution-bias-correction algorithm: enhancing low-resolution and depleting high-resolution reflections is just the effect of the Fourier transform of the ripple distribution, and therefore both concur to a more accurate peak location.

3. Resolution-bias correction beyond RES

In accordance with §2, the minimization of the ripple effects in the electron-density map requires the modification of the scattering factors. In particular, each f'_j is modified so as to reduce the experimentally unobserved fraction of scattering power (*i.e.*, the area below the f_j curve and beyond RES). The algorithm increases the scattering power at low resolution, in order to provide peaks in good contrast with the background of the electron-density map. However, even after the resolution-bias correction, a fraction of the scattering power (that beyond RES) is still overlooked: as a consequence, some residual ripples will still affect the electron-density map. The above drawback may be overcome by observing that, even if the geometric characteristics of $\zeta_{[B]_\zeta}$ (*i.e.*, frequency, intensity and location of the ripples) depend only on RES, its Fourier transform $f_{[B]_\zeta}$ does not vanish beyond RES. This permits its use not only for measured, but also for unmeasured reflections. It may then be advisable to calculate the right-hand sides of equations (7) also for higher-resolution reflections.

The calculations are performed as follows. Reflection indices from RES up to a chosen higher-resolution limit, say 1 Å, are generated, to which vanishing $|F|$ moduli are associated. An atom (representative of the jth atomic species) is located at the origin of the unit cell: then the function $\zeta_{j[B]_\zeta}$ obtained at the experimental RES is Fourier transformed up to 1 Å to obtain $f_{j[B]_\zeta}$. The calculation is repeated for each atomic species.

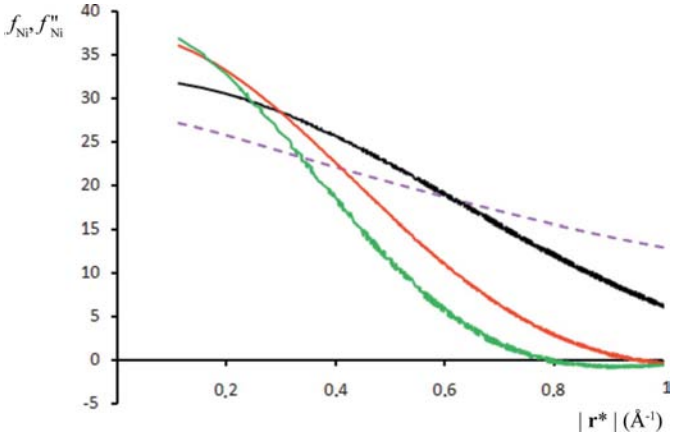

Figure 4
f_{Ni} (at $B = 0$) (dashed purple line). The black line represents f''_{Ni} when RES = 1.0 Å. f''_{Ni} extended to 1 Å resolution from RES = 1.8 and 1.5 Å are represented by a green and a red line, respectively.

In Fig. 3 $f_{Ni[B]_\zeta}$ is extended from RES = 1.8 and 1.5 Å up to 1 Å resolution (the green and red lines, respectively): for comparison we also show the $f_{Ni[B]_\zeta}$ black line when RES = 1.0 Å. The extended lines have a discontinuity at $|\mathbf{r}^*| = 1/\mathrm{RES}$: beyond this point $f_{Ni[B]_\zeta}$ continuously increases with $|\mathbf{r}^*|$. In Fig. 4 the resultant f''_{Ni} curves, extended up to 1.0 Å resolution, are plotted *versus* $|\mathbf{r}^*|$ (in green and red for RES = 1.8 and 1.5 Å, respectively). For comparison we also plot f''_{Ni} when RES = 1 Å (black line) and the true f_{Ni} curve (dashed line). In Appendix *A* it is shown that the discontinuity in the $f_{Ni[B]_\zeta}$ curve is the necessary condition for securing the continuity in the extrapolation of f''_{Ni} beyond RES.

It is worth noticing that the extrapolation of the $f_{j[B]_\zeta}$ to 1 Å is not equivalent to the use of the experimental reflections up to 1 Å. Indeed, in the first case we extrapolate to 1 Å the Fourier transform of the ripple function corresponding to the experimental RES and correct for the resolution bias; in the second case we execute a structure-factor calculation to 1 Å resolution, without applying the resolution-bias-correction algorithm. The applications will show that better results are obtained in the first case.

4. The effects of the temperature factor on the resolution bias

If for a given crystal structure all the scattering factors naturally vanish at the experimental RES, then the truncation effects on the electron density also vanish. Indeed, under these conditions, equation (1) reduces to an identity, $F'_{\mathbf{h}} = F_{\mathbf{h}}$. A physical factor intrinsically reducing the resolution bias is the temperature factor B: when $B \neq 0$ Å^2 the overall scattering power beyond a given RES is smaller than at $B = 0$ Å^2, and therefore smaller resolution-bias effects on the electron density are expected. However, in contrast with the resolution-bias correction, the electron-density peak will show a smaller contrast with the background.

To involve the thermal factor in the algorithm the following equation is used instead of equation (8):

$$F''_{\mathbf{h}} = \sum_{j=1}^{N} [(f_j^o)' - f_{j[B]_\zeta \mathbf{h}}] \exp(-B|\mathbf{r}^*|^2/4) \exp(2\pi i \mathbf{h} \cdot \mathbf{r}'_j), \qquad (9)$$

where f_j^o is the scattering factor of the jth atom at rest.

5. Cycling the algorithm

Equations (7)–(8) had already been obtained in paper I, but they were never applied because the authors were not sure how useful such equations were. In the following we explain why. Let us suppose that, from experimental data at resolution RES, an electron density $\rho'(\mathbf{r})$ is available from which a structural model (in terms of atomic positions $\mathbf{r}'_j$ and thermal factors B_j) is derived. Since $\rho'(\mathbf{r})$ is affected by resolution bias, a new electron density [say $\rho''(\mathbf{r})$] may be calculated by using the structure factors $F''_{\mathbf{h}}$ given by equation (8) as Fourier

coefficients. The electron density $\rho''(\mathbf{r})$ is expected to be less affected by resolution bias: in practice, its peaks are expected to be located on better positions. In paper I, the authors guessed that, even if equations (7)–(8) are able to reduce the ripples, they are expected to introduce new ripples in $\rho''(\mathbf{r})$ corresponding to the 'pseudo-atoms' related to the modified scattering factors.

This belief has been checked in our applications (see §6): it was confirmed, but the ripples in $\rho''(\mathbf{r})$ are less biased than in $\rho'(\mathbf{r})$. This result suggests that the algorithm may be repeated more times: *i.e.*, the modified atomic scattering factors may be modified further by the same algorithm, so as to obtain structural models more and more free from resolution bias.

To describe the cycling process better let us suppose that we have already performed the first cycle of the algorithm: *i.e.*, we have already obtained, through the structure factors defined by equation (9), an improved electron density $\rho''(\mathbf{r})$. Then, for each jth atomic species, a representative atom is moved to the origin of the unit cell and the structure factors of this substructure are calculated by using $f_j''' = (f_j' - f_{j[B]_\zeta \mathbf{h}})$ as a scattering factor. The corresponding electron density will show, besides the main peak at the origin, the corresponding ripples (expected to be smaller than those in the first cycle): their Fourier transform will now be subtracted from f_j''. When all the above calculations have been made for each atomic species, then a new electron density $\rho''(\mathbf{r})$ is calculated, which is expected to show a better ratio between main peaks and ripple intensities.

6. The first applications

To check this theory we used two simulated examples and one real case. The first example aims to show the effects of the algorithm on the ripples of an isolated atom. The second uses a small simulated structure to study the reciprocal effects of the ripples on the atomic positions, and the effects of the algorithm on the experimental electron-density map. The third example uses a well refined real structure whose electron density is deformed by the ripples. The effects of the algorithm on such a map are described at different RES values.

(*a*) We placed an Ni atom at the origin of a unit cell, and calculated the ratios between the main peak intensity (I_{MP}) and the intensities of the first positive (I_{FPR}) and negative ripple (I_{FNR}) before and after the resolution-bias correction [that is, in $\rho'(\mathbf{r})$ and $\rho''(\mathbf{r})$, respectively]. In Table 1 we show I_{MP}, I_{FNR}, I_{FPR} and the ratios I_{MP}/I_{FNR} and I_{MP}/I_{FPR} at different values of RES. The values of I_{MP} after the resolution-bias correction (quoted in parentheses) are slightly smaller than the original values (on average they are 80% of the original values), but the ratios I_{MP}/I_{FPR} and I_{MP}/I_{FNR} are always remarkably larger for the corrected electron density (on average twice as large). The overall result is that $\rho''(\mathbf{r})$ is a cleaner electron density than $\rho'(\mathbf{r})$.

(*b*) In a monoclinic unit cell, with parameters a = 12.39, b = 8.93, c = 8.84 Å, β = 90.55°, space group $P2_1/n$, we placed a regular octahedron having Ni as a central atom and six O atoms as anions (we called this simulated structure NIOCT).

Table 1
Comparison of Ni peak and ripple intensities for canonical and resolution-bias-corrected electron densities.

Values from resolution-bias-corrected electron densities are given in parentheses. Intensities are in arbitrary units.

RES (Å)	I_{MP}	I_{FNR}	I_{FPR}	I_{MP}/I_{FNR}	I_{MP}/I_{FPR}
1.0	687 (580)	43 (22)	20.0 (8.8)	16.0 (26.4)	34.4 (65.9)
1.5	252 (206)	21 (10)	9.3 (3.4)	12.0 (20.6)	27.1 (60.6)
1.8	149 (120)	13 (6.4)	6.4 (2.1)	11.5 (18.8)	23.3 (57.1)

Table 2
Positional discrepancies for Ni and anions in NIOCT.

The number of anions at a distance less than 0.6 Å from their true positions are given in parentheses; the information is not given when all the anions are quite well located. All other values are given in angströms.

RES	d'_{Ni}	d''_{Ni}	d'''_{Ni}	$\langle d' \rangle_a$	$\langle d'' \rangle_a$	$\langle d''' \rangle_a$
1.0	0.006	0.005	0.004	0.071	0.044	0.012
1.5	0.011	0.007	0.011	0.175	0.127	0.056
1.8	0.007	0.005	0.029	0.340	0.261 (1)	0.117

Table 3
Comparison of Ni peak and ripple intensities for the canonical electron density and after the cyclic application of the resolution-bias-correcting algorithm.

Values after the cyclic application of the resolution-bias-correcting algorithm are given in parentheses. Intensities are in arbitrary units.

RES (Å)	I_{MP}	I_{FNR}	I_{FPR}	I_{MP}/I_{FNR}	I_{MP}/I_{FPR}
1.0	687 (345)	43 (3.6)	20.0 (0.8)	16.0 (95.8)	34.4 (431.3)
1.5	252 (83)	21 (1.9)	9.3 (0.6)	12.0 (43.7)	27.1 (138.3)
1.8	149 (32)	13 (1.0)	6.4 (0.3)	11.5 (32.0)	23.3 (106.7)

Structure factors were calculated up to RES = 1.8, 1.5 and 1.0 Å, and their moduli were used as observed amplitudes. We computed $\rho'(\mathbf{r})$ at the three RES values: as expected, the coordinates of the main peaks $\mathbf{r}'_j$ do not coincide with the true atomic positions $\mathbf{r}_j$. Owing to the ideality of our tests (*i.e.*, the absence of experimental errors) the positional errors $d'_j = |\mathbf{r}_j - \mathbf{r}'_j|$ may only be attributed to the resolution bias.

Using equation (8) we computed $\rho''(\mathbf{r})$, from which the positional errors $d''_j = |\mathbf{r}_j - \mathbf{r}''_j|$ were derived. In Table 2 we show, for each RES, the discrepancies for Ni (d'_{Ni} and d''_{Ni}) and the average discrepancies for the anions ($\langle d' \rangle_a$ and $\langle d'' \rangle_a$) before and after the resolution-bias correction. In general, the $\mathbf{r}''_j$ positions are closer to $\mathbf{r}_j$ than the positions $\mathbf{r}'_j$, with one exception when RES = 1.8 Å. This case will be discussed below.

The same structures were used to verify the effectiveness of a cyclic bias correction, as described in §5. In our procedure we fixed the maximum number of cycles to 30: the procedure stops when I_{MP}/I_{FPR} and I_{MP}/I_{FNR} become larger than five times their original value.

In Table 3 the values of I_{MP}, I_{FNR}, I_{FPR}, I_{MP}/I_{FNR} and I_{MP}/I_{FPR} before and after the application of the cyclic procedure to the Ni structure are given. As expected, I_{MP} progressively

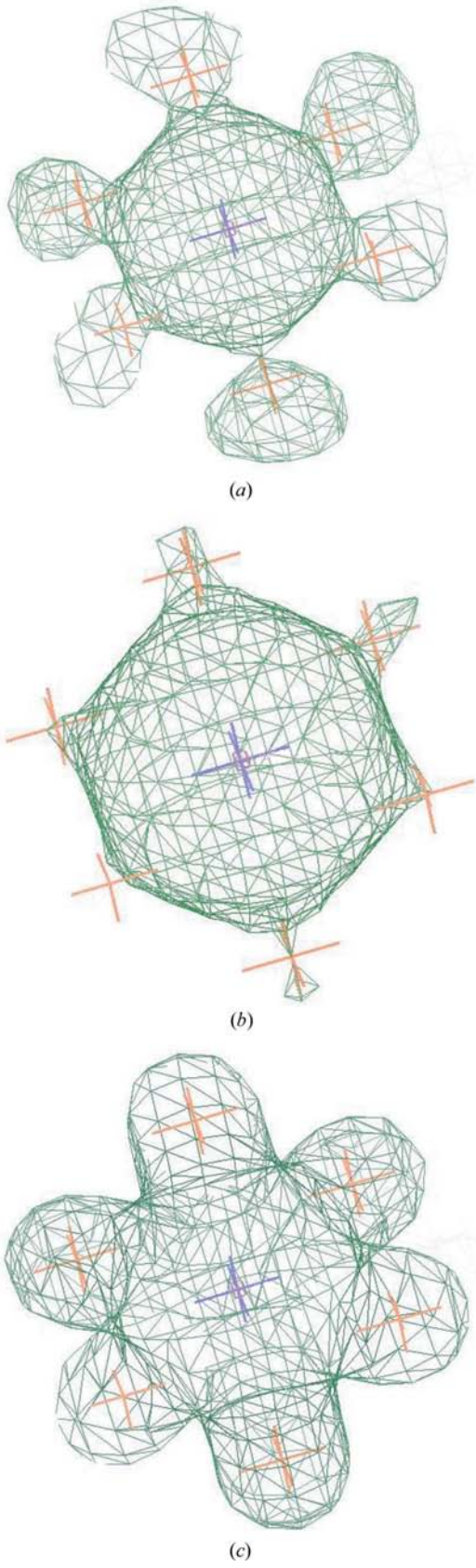

Figure 5
NIOCT at RES = 1.8 Å: (*a*) $\rho'(\mathbf{r})$; (*b*) $\rho''(\mathbf{r})$ after one cycle of resolution-bias correction; (*c*) $\rho'''(\mathbf{r})$ after several cycles of resolution-bias correction.

decreases with the cycle number, but the ripple intensities decrease faster, thus giving rise to augmented ratios I_{MP}/I_{FPR} and I_{MP}/I_{FNR}. The improvement diminishes with RES.

The corresponding positional discrepancies obtained for NIOCT at the end of the cyclic procedure are added in Table 2 as d'''_{Ni} and $\langle d''' \rangle_a$, respectively. It may be seen that the cyclic application of the bias correction provides a better location of the atomic positions and a well behaved background.

Let us now discuss the seemingly dissonant result for $\langle d'' \rangle_a$ obtained when RES = 1.8 Å: *i.e.*, the program is not able to find more than two peaks in the electron density, the first related to the Ni position and the second to an O-atom position. This may be explained as follows: in accordance with §2, the resolution-bias correction sharpens the scattering factors and consequently broadens the electron-density peaks. When RES = 1.8 Å the modified peaks strongly overlap: in our case the stronger Ni-atom peak conceals the O-atom peaks. To better understand the effects, the electron-density map of NIOCT at RES = 1.8 Å is shown in Fig. 5(*a*), as calculated by using the canonical scattering factors. Figs. 5(*b*) and (*c*) show the corresponding maps calculated when the resolution-bias correction is carried out by one cycle or by the cycled procedure. In all cases only the map intensity values larger than 2σ are plotted. The crosses mark the true positions of the atoms (obviously, Ni corresponds to the central peak in each map). We note:

(i) in Fig. 5(*a*) the O-atom positions are within the selected electron density, but are clearly displaced from their correct positions;

(ii) in Fig. 5(*b*) the Ni-atom peak hides the O-atom peaks;

(iii) in Fig. 5(*c*) the Ni-atom intensity is reduced by the algorithm, the light atom peaks are no longer concealed and occupy more correct positions. In some way, recycling the algorithm tends to compensate the broadening effect and leads to a well resolved map.

It is clear from the above results that the data resolution, thermal factor and phase error are limiting factors for the resolution-bias-correction algorithm. Low data resolution may: (i) conceal peaks, which are therefore neglected by the algorithm (*i.e.*, their ripples are not eliminated); (ii) cause partial overlapping of bound atoms: the peaks are then centred on shifted positions, with a consequent shift of the ripple distribution; (iii) severely misplace peak positions as an effect of the ripples of other peaks. In (ii) and (iii) $\mathbf{r}'_j$ strongly differs from $\mathbf{r}_j$ and the ripple correction will show positional bias. Low-resolution effects are particularly severe when bond distances are small and/or when light atoms are close to heavy atoms. The results described above indicate that RES = 1.8 Å may be considered a reasonable limit for the algorithm.

The thermal agitation broadens the atomic electron density. When only a rough structural model is available, B is not known with sufficient accuracy, and the ripple correction may suffer by a positional bias.

If the phase error is high, the percentage of false and/or misplaced peaks is high: in this case correcting ripples of a false molecular model cannot lead to the correct structure.

Table 4
Numerical values of the criteria evaluating the quality of the electron-density maps for SELEN before and after the application of the resolution-bias-correction algorithm to ρ' density maps computed with correct phase values.

The symbols are defined in the text. Values obtained using equation (9) are given in parentheses.

RES (Å)	N_d	$\langle d \rangle$ (Å)	$I_{\rm LAST}/I_{\rm WRONG}$
1.0	25 (25)	0.053 (0.038)	2.1 (4.3)
1.5	21 (21)	0.168 (0.124)	1.6 (4.8)
1.8	18 (19)	0.249 (0.212)	2.0 (6.6)

In spite of the above limitations, the resolution-bias algorithm proved to be highly useful when applied to structure solution from powder data: average phase errors less than 45° and RES better than 1.6 Å still allow fruitful use of the algorithm (see paper II).

We have also checked the usefulness of the resolution-bias correction beyond RES (see §3). For the sake of brevity we only give the numerical result for NIOCT when RES = 1.8 Å and the resolution-bias correction is extended up to 1 Å. Then $d'''_{\rm Ni}$ = 0.003 Å and $\langle d''' \rangle_{\rm a}$ = 0.021 Å. These values may be usefully compared with those obtained from an electron-density map directly computed by using the calculated structure factors up RES = 1 Å. We have $d'_{\rm Ni}$ = 0.006 Å and $\langle d' \rangle_{\rm a}$ = 0.071 Å, remarkably larger than the values obtained by our algorithm.

(*c*) The crystal structure of (2*S*,6a*R*,10a*R*)-6,6,9-trimethyl-1-oxo-2-phenylseleno-1,2,3,4,6a,7,8,9,10,10a-decahydro-6*H*-dibenzo[*b*,*d*]pyran (referred to from now on as SELEN), (Clegg *et al.*, 1980), with 25 non-H atoms in the asymmetric unit, space group $P2_1$, a = 10.30, b = 9.92, c = 10.84 Å and β = 114.62°, was used as a typical example encountered in practice. The structure was originally solved using single-crystal data with RES = 0.8 Å and a final crystallographic residual R_1 equal to 0.05, calculated over 2388 symmetry-independent reflections with $|F|$ larger than $4\sigma(|F|)$. From the published crystallographic coordinates the structure factors were calculated at 1.0, 1.5 and 1.8 Å resolution: the corresponding phases were used for computing observed electron-density maps [$\rho'(\mathbf{r})$ in our notation]. Owing to the resolution bias the atom positions moved from their correct positions so providing distorted models of the structure. The map quality may be analysed by means of the following criteria (see Table 4): (i) the number of peak positions in the asymmetric unit, N_d, which are displaced from the true positions by less than 0.6 Å; (ii) the corresponding average distance $\langle d \rangle$; and (iii) the ratio between the peak intensities corresponding to the last (almost) correctly positioned atom and to the first wrong peak ($I_{\rm LAST}/I_{\rm WRONG}$).

We then computed new electron-density maps by using, as Fourier coefficients, the structure factors obtained *via* equation (9): the results are quoted in Table 4 in parentheses. All the indicators are better when the resolution-bias algorithm is applied: in particular the smaller values of $\langle d \rangle$ suggest that the peaks are better positioned and the largest values of the ratio ($I_{\rm LAST}/I_{\rm WRONG}$) suggest that the corresponding electron-density maps are less noisy.

7. Conclusions

A new algorithm for minimizing the resolution bias in electron-density maps *via* reciprocal-space techniques has been described. The modifications are resolution dependent, and are designed to reduce the ripple intensities in the electron-density maps by increasing the atomic scattering at low diffraction angles and by diminishing it at high angles. A new electron-density map is computed using the calculated structure factors as coefficients. The new map provides more correct atomic positions and a lower background level. It may be argued that, as in the case for the related algorithm for reducing the resolution bias *via* direct-space techniques (see paper II), it may find useful applications both in phasing and in refinement steps.

APPENDIX *A*

Let us suppose that the electron-density map for a one-atom (located on the origin) structure has been calculated by using reflections up to RES. The general unique peak, comprising the main peak $\rho''(\mathbf{r})$ and the ripple function $\rho'_{[B]}(\mathbf{r})$, will be centred on the origin as well:

$$\rho'(\mathbf{r}) = \rho''(\mathbf{r}) + \rho'_{[B]}(\mathbf{r}).$$

By hypothesis the Fourier transform $f'(\mathbf{r}^*)$ vanishes for $|\mathbf{r}^*| > 1/\text{RES}$. This does not occur for $f''(\mathbf{r}^*)$ and for $f_{[B]_\zeta}$: in particular, for $|\mathbf{r}^*| > 1/\text{RES}$, $f_{[B]_\zeta} = -f''(\mathbf{r}^*)$. Thus the discontinuity in the function $f'(\mathbf{r}^*)$ guarantees the continuity of the $f''(\mathbf{r}^*)$ curve.

References

Altomare, A., Caliandro, R., Camalli, M., Cuocci, C., Giacovazzo, C., Moliterni, A. G. G. & Rizzi, R. (2004). *J. Appl. Cryst.* **37**, 1025–1028.
Altomare, A., Cuocci, C., Giacovazzo, C., Kamel, G. S., Moliterni, A. & Rizzi, R. (2008). *Acta Cryst.* A**64**, 326–336.
Altomare, A., Cuocci, C., Giacovazzo, C., Moliterni, A. & Rizzi, R. (2008). *J. Appl. Cryst.* **41**, 592–599.
Booth, A. D. (1946). *Proc. R. Soc. Ser. A*, **188**, 77–92.
Clegg, W., Harms, K., Sheldrick, G. M., von Kiedrowski, G. & Tietze, L.-F. (1980). *Acta Cryst.* B**36**, 3159–3162.
Cruickshank, D. W. J. (1949). *Acta Cryst.* **2**, 65–82.
David, W. I. F., Shankland, K., Cole, J., Maginn, S., Motherwell, W. D. S. & Taylor, R. (2001). *DASH User Manual.* Cambridge Crystallographic Data Centre, Cambridge, UK.
Doyle, P. A. & Turner, P. S. (1968). *Acta Cryst.* A**24**, 390–397.
Rees, B. (1976). *Acta Cryst.* A**32**, 483–488.